Available online at www.sciencedirect.com
SCIENCE DIRECT®
Earth and Planetary Science Letters 241 (2006) 271–280
EPSL
www.elsevier.com/locate/epsl

Evidence from P-to-S mantle converted waves for a flat "660-km" discontinuity beneath Iceland

Z. Du [a], L.P. Vinnik [b], G.R. Foulger [c,*]

[a] Scott Polar Research Institute, University of Cambridge, Cambridge CB2 1ER, UK
[b] Institute of Physics of the Earth, Moscow, Russia
[c] Department of Earth Sciences, University of Durham, Durham, DH1 3LE, UK

Received 4 June 2004; received in revised form 26 April 2005; accepted 19 September 2005
Available online 22 November 2005
Editor: R.D. van der Hilst

Abstract

Iceland is the type example of a ridge-centered hotspot. It is controversial whether the seismic anomaly beneath it originates in the lower mantle or the upper mantle. Some recent studies reported that the 660-km discontinuity beneath central Iceland is shallow relative to peripheral regions and this was interpreted as an effect of elevated temperature at that depth. We investigate topography of the major upper mantle discontinuities by separating the effects of the topography and volumetric velocity heterogeneity in P receiver functions from 55 seismograph stations. Our analysis demonstrates that a significant (at least 10-km) shallowing of the 660-km discontinuity is only possible in the case of improbably low seismic velocities in the mantle transition zone beneath central Iceland. If, as in previous studies, lateral velocity variations in the mantle transition zone are neglected, the data require a depressed rather than an uplifted 660-km discontinuity. For a reasonable S-wave velocity anomaly in the mantle transition zone (around −3%) no topography on the 660-km discontinuity is required. This can be explained by the lack of temperature anomaly or an effect of two phase transitions with opposite Clapeyron slopes.

Keywords: transition zone; receiver functions; Iceland; plume; mantle

1. Introduction

Iceland is widely assumed to be underlain by a mushroom-shaped plume that originates in the deep mantle, perhaps near the core–mantle boundary [1]. However, a deep mantle origin of the seismic low-velocity body beneath Iceland is disputed [2,3]. The magnitude and depth extent of the low-velocity anomaly beneath Iceland have been explored by a number of seismic studies (e.g., [3–11]). Seismic studies using regional teleseismic tomography find in the upper mantle beneath the center of the island a region about 200 km across, where S and P velocities are lower than beneath peripheral areas [5,7–9]. Regional teleseismic tomography using recordings solely from seismograph stations on land in Iceland can only resolve structure in the depth range between about 100 and 400 km. The structure at depths exceeding 400 km is accessible only using global seismic tomography which has lower lateral resolution [10,11]. These studies suggest that the low-velocity anomaly beneath Iceland extends into the mantle transition zone (MTZ) bounded by the global discontinuities at depths of about 410 km and 660 km.

* Corresponding author.
E-mail address: gfoulger@usgs.gov (G.R. Foulger).

0012-821X/$ - see front matter © 2005 Elsevier B.V. All rights reserved.
doi:10.1016/j.epsl.2005.09.066

The interior of the Earth can also be imaged using receiver function techniques based mainly on the use of either P-to-S (Ps) or S-to-P (Sp) converted phases (e.g., [12]). The arrival times of the converted phases are sensitive to the depths of conversion and can be used to infer topography on the discontinuities. The major mantle discontinuities are explained as phase transitions and their depths can be interpreted in terms of temperature. The discontinuities at depths of about 410 km and 660 km are attributed, respectively, to isochemical phase transformations from olivine to wadsleite with a positive Clapeyron slope, and from spinel to perovskite and magnesiowustite with a negative Clapeyron slope [13,14]. The structure near 660 km depth is complicated by the transition from majorite garnet to perovskite in the pyroxene component [15], which has a positive Clapeyron slope.

The depths of the major mantle discontinuities beneath Iceland have been inferred from P receiver functions. It has been reported [16,17] that the upper discontinuity is depressed beneath south-central Iceland by about 15 km, and the lower discontinuity is uplifted by about the same amount. Such topography is consistent with a temperature anomaly of 100–200 °C throughout the MTZ. Shallowing of the lower discontinuity could be explained by high temperature at the base of the MTZ, and this was taken as evidence that the low-velocity mantle anomaly, which was assumed to represent a hot plume, extends into the lower mantle. However, a flaw in this analysis is neglect of the effects of volumetric velocity heterogeneity in the mantle beneath Iceland. Strong lateral heterogeneity is demonstrated by numerous seismic studies, and its effects upon the travel times of converted phases are comparable in magnitude to the effects of the discontinuity topography. Our present analysis differs from previous work in that we consider the effects of volumetric velocity heterogeneity in estimating the discontinuity topography.

In addition to shallowing of the 660-km discontinuity, the most recent P-receiver function study [18] even claims to resolve a tilt of a few tens of degrees of a columnar low-velocity body beneath central Iceland. Such a tilt has not been recognized yet in existing tomography models in the depth range where resolution is good. We conducted an exhaustive search for seismic recordings sensitive to such a tilt using a larger data set than in [18], but found only a few suitably located wave paths. The receiver functions obtained from those seismograms are too few and noisy to yield meaningful results. We conclude that the presently existing data have insufficient resolution to distinguish any deviation of the low-velocity body from vertical.

2. Method and data

A *P* receiver function is the response of the Earth in the vicinity of a seismograph station to excitation by teleseismic P waves. P-to-S converted phases provide the most informative part of this response. In our analysis we use the method described in [19]. The initial seismogram is decomposed by axis rotation into three components, P, SV and T. The P component is parallel to the principal direction of P-wave particle motion in the wave-propagation plane. The SV component is perpendicular to the P component in the same plane and is optimal for detecting the Ps converted phases. Recordings of different seismic events are equalized by deconvolving them using the P components. In our study, deconvolution is performed in the time domain with proper regularization. To extract weak converted phases from noise, the individual deconvolved SV components are stacked with move-out time corrections. The corrections and related stacks are calculated for several assumed depths of conversion. The reference slowness (the slowness that does not require move-out corrections) is fixed at 6.4 s/deg. as in other similar studies. The depth of conversion is determined from the time of the Ps phase (the delay relative to the P phase). The largest amplitude of this phase should occur on the trace appropriate to that depth. This is a criterion to distinguish between the true converted phases and signal-generated noise that is caused mainly by reverberations in the upper layers.

We used seismograms recorded at 55 broadband digital stations in Iceland (Fig. 1). The stations belong to the permanent SIL network and the temporary ICEMELT and Iceland Hotspot Project networks [6,7,20]. The severe microseismic noise in Iceland was suppressed by low-pass Butterworth filtering with a corner period of about 6 s. Large earthquakes (magnitude >5.8) suitable for our study occur in many regions. Most of the suitable seismograms lie in the epicentral distance range of 45–94°. Over 6000 individual seismograms were examined, from which 500 of the best were used (Table 1). The SV components of the individual receiver functions were normalized to the peak in the P component of the deconvolved P waves. The maximum amplitude of noise in the selected individual receiver functions in the time window of interest is less than 0.1, whereas typical amplitudes of the mantle Ps phases are about 0.03. The individual receiver functions were divided into a few groups containing more than 70 functions each and stacked to reduce noise. In every group three Ps phases were detected with confidence: the crustal phase at a time of about 2.5 s and the two

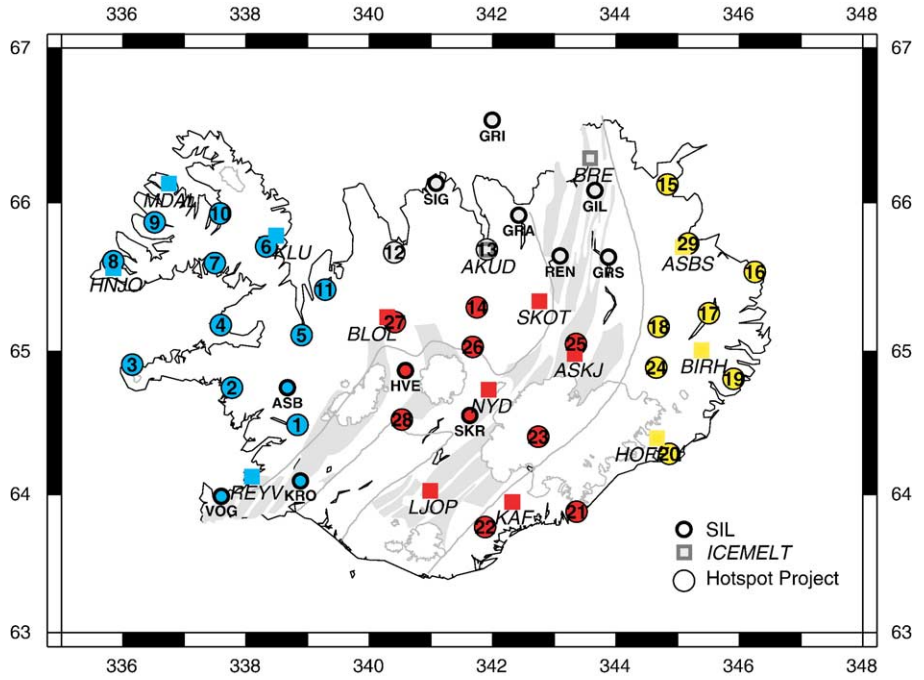

Fig. 1. Map of Iceland showing surface tectonic features, icecaps (white) and seismic stations used. Stations in the eastern, western and central regions are shown as yellow, blue and red, respectively. SIL: permanent stations of the Icelandic network. ICEMELT and Hotspot Project indicate temporary stations.

phases from the major mantle discontinuities at depths of about 410 km and 660 km. The crustal phase corresponds to a discontinuity within the crust at about 15–20 km depth. This discontinuity is known from previous studies (e.g., [21]). The signal from the crust–mantle boundary arrives in the midst of other late arrivals and cannot be detected. Bootstrap analysis [22] shows that the times of the major mantle phases are determined with an RMS error of about 0.2 s. The differences between the times of these phases in a single stack are determined with an RMS error of about 0.3 s. This means that variations in the times of the order of 1 s are statistically significant.

To take into account lateral velocity heterogeneity in the upper ~400 km beneath Iceland, as shown by regional teleseismic tomography, we divide Iceland into three parts, each of which can be regarded to be laterally homogeneous to a first approximation. These are central, east and west Iceland. The eastern and western regions correspond to the Eurasian and American plates, respectively, and lie outside the strongly anomalous central region. The groups of stations in different regions are shown in Fig. 1 in different colors. To ensure that the wave paths of the Ps phases in the east and west lie outside the central region, we stacked receiver functions for seismic events mainly in the azimuths clockwise from 0° to 180° for the eastern group and from 180° to 360° for the western group. For the central region we assembled two stacks as described in Section 4.

We also attempted to assemble sets of seismograms sampling the regions to the north and south of the

Table 1
Times, in seconds, of P410s and P660s and differential times for the receiver function stacks discussed in the text

	Western region	Eastern region	Average W and E (the peripheral region)	IASP91	Central region Stack-410	Central region Stack-660
Time, P410s	47.3	46.9	47.1	44.0	50.5	48.6
Time, P660s	71.5	70.1	70.8	67.9	73.0	72.8
Differential time	24.2	23.2	23.7	23.9	22.5	24.2
Number of stacked receiver functions	199	104			124	73

central region. However, these sets, in contrast to the others, were too heterogeneous to yield clear results. In particular, the wave paths to the south sample the southern margin of the central region, the Mid-Atlantic Ridge and both plates; deep structure beneath the ridge is very different from that beneath the plates [23]. The effects of lateral velocity variations and of topography of the discontinuities are practically inseparable in this data set. A similar complexity in the north is complemented by a weakness of the Ps phase from the 410-km discontinuity.

3. Results for peripheral regions

The receiver function stacks are shown in Figs. 2 and 3 and the related travel times of the mantle phases are listed in Table 1. The average differential time for the two regions, collectively termed the peripheral region, is 23.7 s, close to the differential time of 23.9 s for the standard global model IASP91 [24]. The standard differential time is nearly identical to the average for the global seismograph network [25]. The structure of the MTZ beneath the peripheral region is thus either similar to the global average or the effects of anomalous thickness and velocity cancel out in the differential time. The latter explanation is least likely (see the discussion in Section 5), and therefore we adopt the first option as has been done elsewhere [26]. The deviations in travel time of the related Ps phases from the standard time must then be attributed to the properties of the mantle at depths less than 410 km. The deviations, Δt_{Ps}, are 3.1 s for the 410 km Ps phase and 2.9 s for the 660 km phase. These values are approximately equal to the difference between the residuals Δt_S and Δt_P of the teleseismic S and P phases relative to the standard model, i.e., $\Delta t_{Ps} \simeq \Delta t_S - \Delta t_P$.

Defining $k = \Delta t_S / \Delta t_P$, the ratio between the teleseismic S and P residuals, we may write $\Delta t_S = (1 + 1/(k-1))\Delta t_{Ps}$. The residuals thus obtained are absolute, i.e., calculated with respect to the known velocity model. By comparison, the residuals for regional teleseismic tomography are usually calculated relative to their average values for the region, whereas the absolute residuals are unknown. The theoretical value of k for the upper mantle with a low anelastic attenuation is 2.7 [26]. If attenuation is high (temperature in the mantle is close to the solidus temperature) the value of k can be higher. The upper limit for observed k is ~3.8, the value obtained by comparing teleseismic P and S residuals and by combined analysis of P residuals and the travel times of Ps phases from the major discontinuities in western North America [26]. The residuals in the peripheral region of Iceland are comparable to those in western North America. For $k = 3.8$ and $\Delta t_{Ps} = 3$ s we

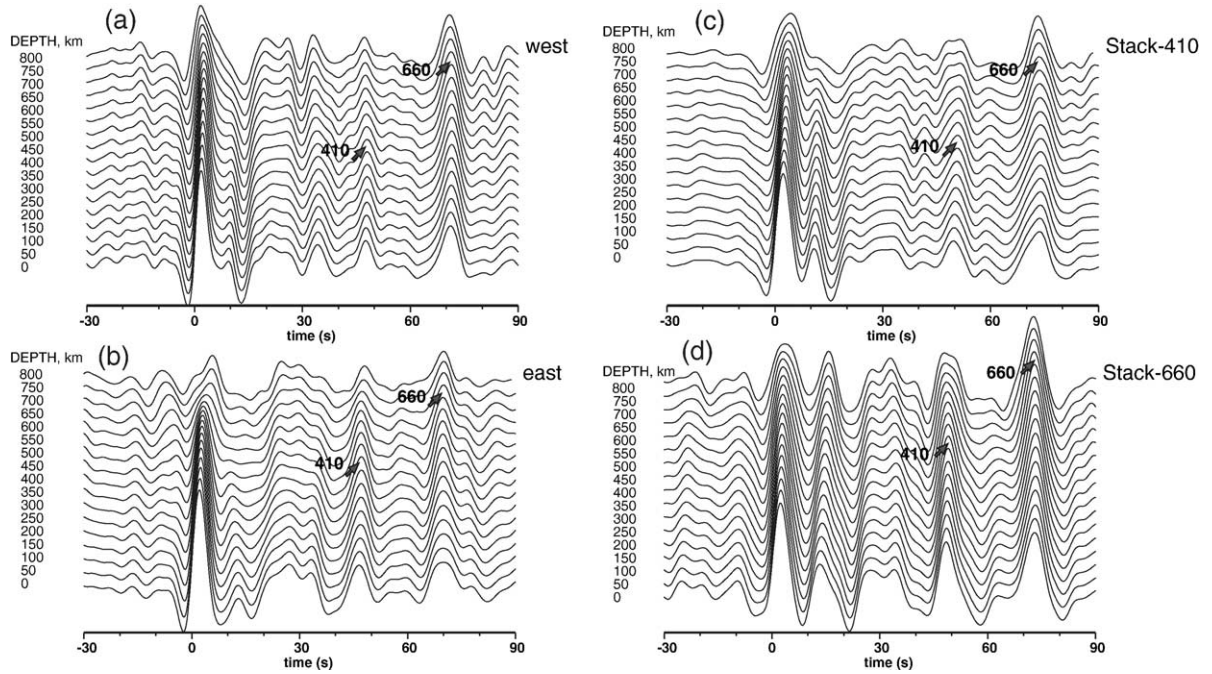

Fig. 2. Stacks of receiver functions. Each trace is a single stack, computed using theoretical move-out corrections appropriate for Ps conversion at the depth specified. Stacks shown are for (a) the western region, (b) the eastern region, (c) Stack-410 of the central region and (d) Stack-660 of the central region. Origin of the time scale corresponds to the arrival of the P wave. The P410s and P660s are marked by arrows.

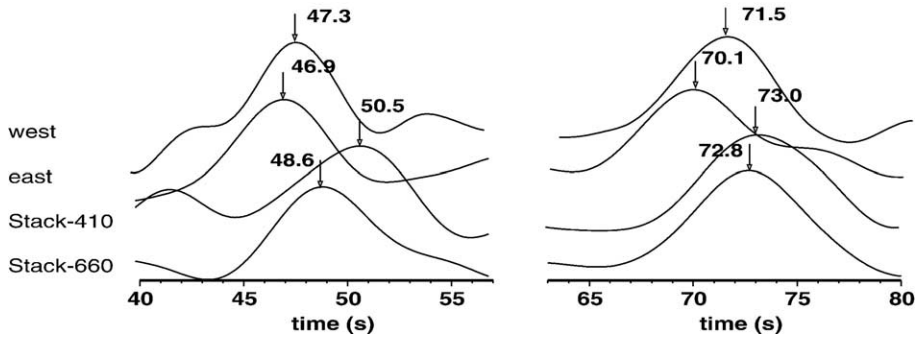

Fig. 3. Expanded parts of the receiver function stacks showing the P410s (left panel) and P660s (right panel) phases. Phases for the west, east, center Stack-410 and center Stack-660 are shown.

obtain $\Delta t_S = 4$ s. This is the lower limit of the S residual that can be inferred from our data. This value can be compared with the model [9] based on the phase velocities of Love surface waves in Iceland. In this model the S-wave velocity in the peripheral regions in the depth range 50–220 km changes linearly from −10% to 0%. The average velocity anomaly in this model is thus close to −5%. From our data the average anomaly in the same layer can be obtained from $\Delta V_S/V_S = \Delta t_S/t$, where V_S and t, the average S-wave velocity and the average travel time, are 4.5 km/s and 38 s, respectively. The corresponding value of the S-wave velocity anomaly ΔV_S is then −10%, which is twice that obtained in [9]. The anomaly could be weaker than −10% but extend to a greater depth.

4. Results for the central region

The deep structure of the central region is the primary target of this study. To investigate this we assembled two stacks of receiver functions, and refer to them as Stack-410 and Stack-660, respectively.

4.1. Stack-410

This stack (Fig. 2c) comprises seismograms recorded at stations within the central region, with the corresponding wave paths of the P410s (Ps converted at the 410-km discontinuity), lying within the central low-velocity body. Most of the piercing points (points of conversion) of the P660s lie well outside the central region (Fig. 4a). Only a small number of piercing points of P660s, about 20% of the total, lie close to the outer edge of the central region. Since the wave paths of the P410s are entirely within the central low-velocity body, the inclusion or exclusion of the seismograms with marginal P660s piercing-point locations has no effect on the P410s arrival time, whereas the effect on the time of the P660s (of the order of 0.1 s) is insignificant. The differential time between the P660s and P410s in this stack is 22.5 s, 1.4 s less than for the IASP91 model. The time of the P410s is 50.5 s, which is 6.5 s longer than the IASP91 time and 3.4 s longer than the corresponding time for the peripheral region. One of the reasons for the large delay relative to the peripheral region is obvious: the wave paths of the Ps phases of this group pass through the central low-velocity body. We discuss several candidate models of the MTZ in order to explain the reduction of the differential time between P660s and P410s by 1.4 s (Fig. 5).

4.1.1. Model 1

The 410-km discontinuity is depressed by about 15 km in the central region, whereas the depth of the 660-km discontinuity outside the central region is standard. The depth of the 660-km discontinuity in the central region cannot be determined because the piercing points of P660s phases at this depth are mostly outside the central region (Fig. 5a). For this model, 1.4 s of the 3.4 s difference between the times of P410s in Stack-410 and the stacks for the peripheral region are caused by depression of the 410-km discontinuity. The remaining 2 s are caused by decreased seismic velocities in the mantle above 410 km within the central low-velocity body. Using the method described in Section 3, we find the S-velocity anomaly in the central body to be approximately −3%, in agreement with the results of regional teleseismic tomography (e.g. [9]) and in favor of this model.

4.1.2. Model 2

The 410-km discontinuity is flat, but the 660-km discontinuity is uplifted in a region about 400 km

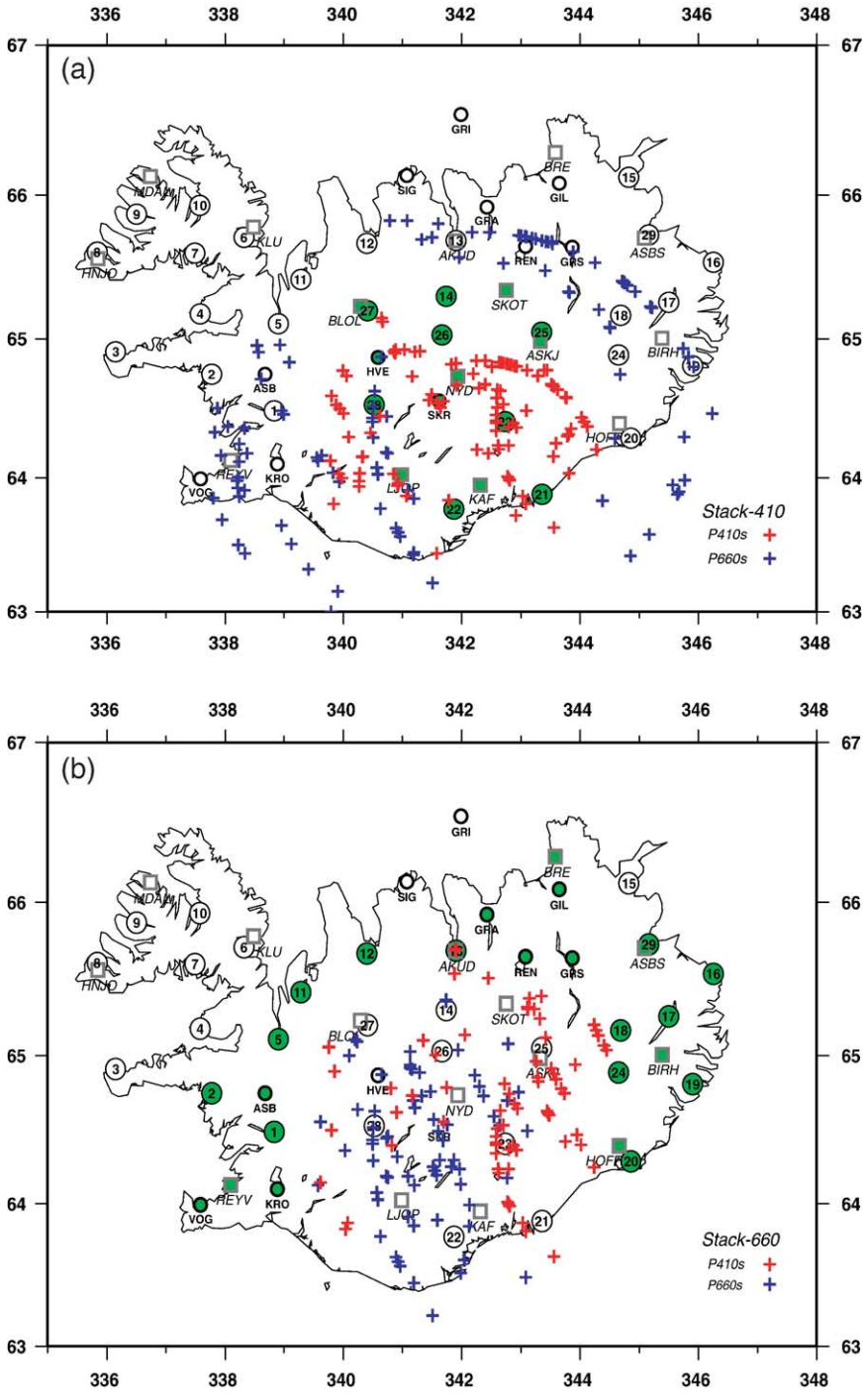

Fig. 4. Projections of piercing points of rays of the converted phases at the 410-km discontinuity (red crosses) and the 660-km discontinuity (blue crosses): (a) Stack-410, (b) Stack-660. The stations used for each stack are shown in green. The calculations were made for the IASP91 model with a slowness of 6.4 s/deg.

wide, much wider than the central region (Fig. 5b). There are two problems with this model. First, such a broad uplift is not supported by the observation of a normal differential time for the two stacks for the peripheral region. This objection is not very critical, however, because most of the rays in the peripheral

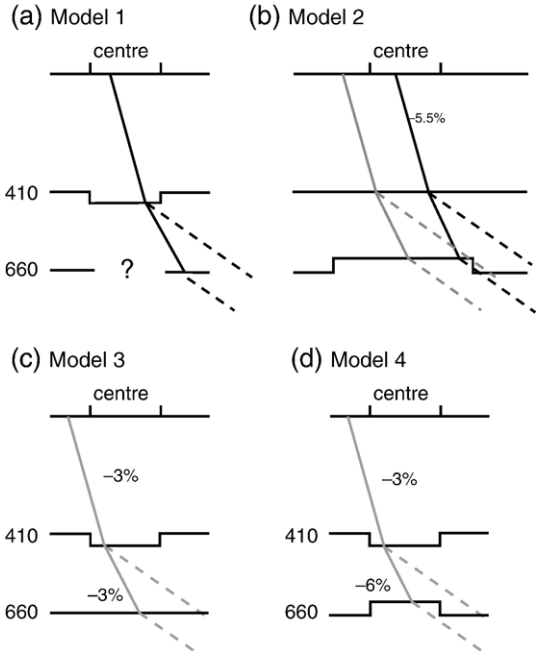

Fig. 5. Sketch illustrating Models 1–4 discussed in the text and wave paths of the Ps phases. Topography on the discontinuities is not drawn to scale. P and S segments of the Ps wave paths are shown by dashed and solid lines, respectively. Wave paths in black correspond to Stack-410 where the receiver is located in the central region and the piercing points at the 410-km and 660-km discontinuities are beneath the central region and outside of it, respectively. Wave paths in grey correspond to Stack-660 where the receiver is located outside of the central region and the piercing points at both discontinuities are beneath the central region. S wave velocity anomalies in % are relative to the peripheral region (at depths less than 410 km) and relative to the standard model (in the MTZ). See Section 4 for more details.

stacks sample the region at a large distance from central Iceland, whereas the region adjacent to the central region is not well sampled. Secondly, if the 410-km discontinuity is not depressed, the above-estimated 3.4 s delay of P410s relative to the peripheral region must be caused entirely by lower velocity above the 410-km discontinuity, and the average S-wave velocity anomaly required in the central region relative to the peripheral region is then about −5.5%. This is about twice that observed in regional teleseismic tomography models [9] (see Section 3 for the method used to calculate the S-wave velocity anomaly). Similar arguments apply to models intermediate between 1 and 2.

If it is assumed that both discontinuities are flat, the reduction in the differential time requires S-wave velocity ~5% high in the MTZ. This is unlikely since global tomography (e.g. [10]) detects, on the contrary, low velocities in the MTZ beneath Iceland.

4.2. Stack-660

For this stack (Fig. 2d), the stations used are located outside the central region, whereas the piercing points at the 660-km discontinuity are located entirely beneath the central region (Fig. 4b). Most of the piercing points at the 410-km discontinuity are also located beneath the central region. A few are outside the central region but close to its boundary. The time of the 410-km Ps phase, 48.6 s, is 1.9 s smaller than for Stack-410, as could be expected, since the wave paths in the upper 410 km lie mostly outside the central low-velocity body. The differential time is 1.7 s larger than for Stack-410. This observation provides evidence against Model 2, because if the 660-km discontinuity in the central region is uplifted a reduction of the time of P660s should be expected, which would, in turn, cause a smaller differential time. Based on this argument and the arguments in the preceding sub-section, Model 2 is regarded improbable.

We consider a few modifications of Model 1 in order to reconcile it with the nearly standard differential time for the second stack. In the differential time we consider the effects (a) of a depression of the 410-km discontinuity, (b) of a velocity anomaly in the MTZ beneath the central region, and (c) of topography on the 660-km discontinuity beneath the central region. We estimate all effects with respect to the standard model IASP91. To obtain the standard differential time, the sum of (a), (b) and (c) should be around 0 s. Many piercing points at the 410-km discontinuity in Stack-660 are within or close to the central region where the discontinuity is depressed, and, if we take this into account, a rough estimate of (a) is about −1 s.

If, as in previous studies [16–18], (b) is neglected, (c) must be about 1 s, and Stack-660 requires a depression of the 660-km discontinuity of about 10 km. Such a depression is the opposite of the elevation proposed in [16–18]. This variant also contradicts the evidence of low S-wave velocity in the MTZ beneath Iceland detected in global tomography models (e.g., [10]).

To evaluate (b), we discuss a few possibilities. In the global tomography model [10] the reduction of the S-wave velocity in the MTZ is about 1.5%, and the corresponding reduction of the P-wave velocity is 0.75%. Assuming that the central low-velocity body extends into the MTZ with a similar width to that observed above the 410-km discontinuity (~200 km), and extends down as far as 660 km, the predicted value of (b) is about 0.5 s. This is probably a lower limit because global tomography tends to underestimate velocity anomalies because of volume averaging. Another

approach to estimating (b) is to use the peak velocity anomalies in the central low-velocity body at depths between 200 and 400 km (4% and 2% for P and S waves, respectively), as given by regional teleseismic tomography [9]. The corresponding value of (b) is then about 1.3 s. This value can be viewed as an upper limit. Therefore, the possible estimate of (b) from tomographic models is in the range ~0.5–1.3 s.

Another approach for evaluating (b) is to calculate the effect of elevated temperature by using the appropriate derivative [27]:

$$\delta \ln V_S / \delta T = -1.35 \times 10^{-4}\ \mathrm{K}^{-1}$$

where T is temperature, and assuming $\delta \ln V_S / \delta \ln V_P = 1.7$. The maximum temperature anomaly in the upper mantle beneath Iceland permitted by seismic data is around 200 K (for a review of temperature estimates see [28]). For this temperature the anomalies in the S-wave velocity and (b) are predicted to be about −3% and 1.0 s, respectively; this value of (b) is intermediate between the upper and the lower limits estimated above.

4.2.1. Model 3

According to the analysis above, (a) and (b) then cancel out, and (c) is 0 s. This means that the 1 s reduction of the differential time due to the depression of 410-km discontinuity is completely balanced in the Stack-660 by the velocity anomaly in the MTZ. Based on this, we prefer Model 3, as shown in Fig. 5c. This model does not require topography on 660-km discontinuity.

4.2.2. Model 4

If the actual reduction in S-wave velocity is near the upper or the lower limit, an uplift or depression of the 660-km discontinuity of a few kilometers is required. But to obtain an elevation of the 660-km discontinuity of 10 km, as suggested in [16,17], the velocity anomalies in the MTZ are required to be about −6% and −3% for S and P waves, respectively. Such a model (Fig. 5d) is unlikely, as the velocity anomaly beneath the 410-km discontinuity is then twice that above it, and there are currently no supporting observations for such a model [10].

To summarize, Model 3 is most consistent with all the available data.

5. Discussion and conclusions

We find that the low-velocity anomaly beneath the peripheral region of Iceland is about twice as large as reported in a summary of regional tomography results [9]. Our result is based on the assumption that the 410-km discontinuity beneath the peripheral region lies at the global average depth defined by IASP91. A comparable result was also obtained from Sp receiver functions [28]. The agreement between the estimates derived independently from both P and S receiver functions suggests that this is a robust result. If the estimate given in [9] is correct, the 410-km discontinuity beneath the peripheral region would have to be ~15 km deeper than the global average. Thinning of the MTZ will decrease the differential time, but we observe a normal differential time for the peripheral region. Therefore, a depression of the 410-km discontinuity would have to be complemented by a negative velocity anomaly in the MTZ of the order of several percent. This is unlikely because a velocity anomaly of such magnitude and lateral extent in the MTZ would be detected by global tomography [10] but to date has not been observed. A depression of both the 410-km and 660-km discontinuities is also unlikely because the downwarping of the MTZ as a whole would produce a large gravity anomaly which is not observed.

The depression of approximately 15 km on the 410-km discontinuity beneath the central region is a robust result. It is consistent with temperature elevated by 100–200 K above the global average at the same depth, depending on how much of the anomaly is caused by compositional variation [29]. Estimates of topography on the 660-km discontinuity beneath Iceland depend on the velocities in the MTZ. In our preferred Model 3 (Fig. 5c) this discontinuity is flat within the resolution of receiver function studies. This requires that the low-velocity body beneath central Iceland extends throughout most of the MTZ, but does not affect its lower boundary. The likely reduction in S-wave velocity in the MTZ is about 3% relative to the standard model, which is consistent with a maximum temperature anomaly of about 200 K or less, if the MTZ is wet. An elevation of 10 km on the 660-km discontinuity, as reported previously, is possible only if the S-wave velocity anomaly in the MTZ attains the improbably high value of −6%.

Regional teleseismic tomography assumes that body-wave travel time residuals result from structure in a limited depth range (in Iceland, less than 400 km) beneath the seismograph network. At greater depths the Earth is assumed to be laterally homogeneous. This assumption is clearly violated beneath Iceland if the low-velocity body extends into the

MTZ. The discrepancy between our estimates of the velocity anomaly beneath the peripheral region and that of [9] most likely occurs also because of (a) relatively low resolution of the surface waves used in [9] and (b) the fact that the teleseismic body-wave residuals used in [9] and the velocity anomalies calculated are relative to the average values in Iceland, whereas our residuals are absolute.

The lack of topography on the 660-km discontinuity is consistent with a zero temperature anomaly beneath Iceland at this depth and an upper mantle origin for the Iceland hotspot. However, other possibilities cannot be ruled out such as the effect of two phase transitions with opposite Clapeyron slopes [15] reducing the sensitivity of depth of the 660-km discontinuity to temperature.

Acknowledgments

This research was supported by Natural Environment Research Council (NERC) Grant GR3/10727 and a Sir James Knott Foundation fellowship held by GRF. LV was supported by RFBR Grant 04-05-64634. Some of the digital seismic data were provided by the IRIS Data Management Centre and the Icelandic Meteorological Office. The authors appreciate the comments from A. Deuss and an anonymous reviewer, who suggested that we discuss Model 2.

References

[1] V. Courtillot, A. Davaillie, J. Besse, J. Stock, Three distinct types of hotspots in the Earth's mantle, Earth Planet Sci. Lett. (2003) 295–308.
[2] D.L. Anderson, The thermal state of the upper mantle; no role for mantle plumes, Geophys. Res. Lett. 27 (2000) 3623–3626.
[3] G.R. Foulger, M.J. Pritchard, B.R. Julian, J.R. Evans, R.M. Allen, G. Nolet, W.J. Morgan, B.H. Bergsson, P. Erlendsson, S. Jakobsdottir, S. Ragnarsson, R. Stefansson, K. Vogfjord, The seismic anomaly beneath Iceland extends down to the mantle transition zone and no deeper, Geophys. J. Int. 142 (2000) F1–F5 (Fast Track).
[4] I.T. Bjarnason, W. Menke, O.G. Flovenz, D. Caress, Tomographic image of the mid-Atlantic plate boundary in southwestern Iceland, J. Geophys. Res. 98 (1993) 6607–6622.
[5] C.J. Wolfe, I.T. Bjarnason, J.C. VanDecar, S.C. Solomon, Seismic structure of the Iceland mantle plume, Nature 385 (1997) 245–247.
[6] F.A. Darbyshire, I.T. Bjarnason, R.S. White, O.G. Flovenz, Crustal structure above the Iceland mantle plume imaged by the ICEMELT refraction profile, Geophys. J. Int. 135 (1998) 1131–1149.
[7] G.R. Foulger, M.J. Pritchard, B.R. Julian, J.R. Evans, R.M. Allen, G. Nolet, W.J. Morgan, B.H. Bergsson, P. Erlendsson, S. Jakobsdottir, S. Ragnarsson, R. Stefansson, K. Vogfjord, Seismic tomography shows that upwelling beneath Iceland is confined to the upper mantle, Geophys. J. Int. 146 (2001) 504–530.
[8] Z. Du, G.R. Foulger, Surface wave waveform inversion for variation in upper mantle structure beneath Iceland, Geophys. J. Int. 157 (2004) 305–314.
[9] R.M. Allen, G. Nolet, W.J. Morgan, K. Vogfjord, B.H. Bergsson, P. Erlendsson, G.R. Foulger, S. Jakobsdottir, B.R. Julian, M.J. Pritchard, S. Ragnarsson, R. Stefansson, Imaging the mantle beneath Iceland using integrated seismological techniques, J. Geophys. Res. 107 (B12) (2002), doi:10.1029/2001JB000595.
[10] J. Ritsema, H.J. van Heijst, J.H. Woodhouse, Complex shear wave velocity structure imaged beneath Africa and Iceland, Science 286 (1999) 1925–1928.
[11] R. Montelli, G. Nolet, F.A. Dahlen, G. Masters, R.E. Engdahl, S.-H. Hung, Finite frequency tomography reveals a variety of plumes in the mantle, Science 303 (2004) 338–343.
[12] V. Farra, L. Vinnik, Upper mantle stratification by P and S receiver functions, Geophys. J. Int. 141 (2000) 699–712.
[13] T. Katsura, E. Ito, The system Mg_2SiO_4–Fe_2SiO_4 at high pressures and temperatures: Precise determination of stabilities of olivine, modified spinel, and spinel, J. Geophys. Res. 94 (1989) 15633–15670.
[14] E. Ito, E. Takahasi, Postspinel transformations in the system Mg_2SiO_4–Fe_2SiO_4 and some geophysical implications, J. Geophys. Res. 94 (1989) 10646–10673.
[15] K. Hirose, Phase transitions in pyrolitic mantle around 670-km depth: implications for upwelling of plumes from the lower mantle, J. Geophys. Res. 107 (2002), doi:10.1029/2001JB000595.
[16] Y. Shen, S.C. Solomon, I.T. Bjarnason, G.M. Purdy, Hot mantle transition zone beneath Iceland and the adjacent mid-Atlantic Ridge inferred from P-to-S conversions at the 410- and 660-km discontinuities, Geophys. Res. Lett. 23 (1996) 3527–3530.
[17] Y. Shen, S.C. Solomon, I.T. Bjarnason, C.J. Wolfe, Seismic evidence for a lower-mantle origin of the Iceland plume, Nature 395 (6697) (1998) 62–65.
[18] Y. Shen, S.C. Solomon, I.T. Bjarnason, G. Nolet, W.J. Morgan, R.M. Allen, K. Vogfjord, S. Jakobsdottir, R. Stefansson, B.R. Julian, G.R. Foulger, Seismic evidence for a tilted mantle plume and north–south mantle flow beneath Iceland, Earth Planet. Sci. Lett. 197 (2002) 261–272.
[19] L.P. Vinnik, Detection of waves converted from P to SV in the mantle, Phys. Earth Planet. Inter. 15 (1977) 39–45.
[20] R. Stefansson, Earthquake prediction research in the south Iceland seismic zone and the SIL project, Bull. Seismol. Soc. Am. 83 (1993) 696–716.
[21] G.R. Foulger, Z. Du, B.R. Julian, Icelandic-type crust, Geophys. J. Int. 155 (2003) 567–590.
[22] B. Efron, R. Tibshirani, Statistical data analysis in the computer age, Science 253 (1991) 390–395.
[23] S. Pilidou, K. Priestley, E. De bayle, O. Gudmundsson, Rayleigh wave tomography in the North Atlantic: high resolution images of the Iceland, Azores and Eifel mantle plumes, Lithos 79 (2005) 453–474.
[24] B.L.N. Kennett, E.R. Engdahl, Travel times for global earthquake location and phase identification, Geophys. J. Int. 105 (1991) 429–466.
[25] S.L. Chevrot, L. Vinnik, J.-P. Montagner, Global scale analysis of the mantle Pds phases, J. Geophys. Res. 104 (1999) 20203–20219.

[26] L. Vinnik, S. Chevrot, J.-P. Montagner, F. Guyot, Teleseismic travel time residuals in North America and anelasticity of the asthenosphere, Phys. Earth Planet. Inter. 116 (1999) 93–103.
[27] S. Karato, Importance of anelasticity in the interpretation of seismic tomography, Geophys. Res. Lett. 20 (1993) 1623–1626.
[28] L.P. Vinnik, G.R. Foulger, Z. Du, Seismic boundaries in the mantle beneath Iceland: a new constraint on temperature, Geophys. J. Int. 160 (2005) 533–538.
[29] D.C. Presnall, Phase Diagrams of Earth-forming Minerals, in Mineral Physics and Crystallography: A Handbook of Physical Constants, American Geophysical Union, Washington, DC, 1995.